Electronic Supplementary Information

Sodium-promoted bimetallic *M*-CoO_x catalysts (*M* = In, Ga, Mo, Mn, and V) for the hydrogenation of CO_2 to C_{2+} hydrocarbons

Zuozheng Liu,[a] Furan Guo,[b] Miao Li,[b] Shican Jiang,[a] Xianjun Lang,*[a] Abhishek Dutta Chowdhury,*[a] and Kang Cheng,*[b]

[a] *College of Chemistry and Molecular Sciences, Wuhan University, Wuhan 430072, China*

[b] *State Key Laboratory of Physical Chemistry of Solid Surfaces, Innovation Laboratory for Science and Technologies of Energy Material of Fujian Province (IKKEM), College of Chemistry and Chemical Engineering, Xiamen University, Xiamen 361005, China*

Experimental Details

Materials and catalyst preparation

Urea (CON_2H_4) was purchased from Aladdin Scientific Corp. Natrium carbonate (Na_2CO_3), Gallium nitrate nonahydrate ($Ga(NO_3)_3 \cdot 9H_2O$), Manganese nitrate ($Mn(NO_3)_2$， 50 wt% in water), Indium nitrate tetrahydrate ($In(NO_3)_3 \cdot 4H_2O$) were purchased from Sinopharm Chemical Reagent Co., Ltd. Ammonium molybdate tetrahydrate ($(NH_4)_6Mo_7O_{24} \cdot 4H_2O$) were purchased from Shanghai Titan Scientific Co., Ltd. Ammonium vanadate (NH_4VO_3) were purchased from Xilong Scientific Co., Ltd. Carbon dioxide (CO_2: H_2: Ar = 24:72:4, 99.9%), Nitrogen (N_2, 99.9%) and Hydrogen (H_2, 99.9%) were purchased from Huian Kote Gas Co., Ltd.

M-CoO_x (M = In, Ga, Mo, Mn, and V) bimetallic oxide catalysts were prepared via a urea-assisted hydrothermal precipitation method. In a typical synthesis process, 4.4 g of $Co(NO_3)_2 \cdot 6H_2O$ and an appropriate amount of the M precursor (the M loading was 1.0 wt% unless otherwise specified) were dissolved in 50 mL of deionized water under magnetic stirring until completely dissolved. Subsequently, 5.4 g of urea (Urea/metal (molar ratio) = 6.0) was added, and the mixture was stirred for another 30 min to form a uniform solution. The resulting solution was transferred into a Teflon-lined stainless-steel autoclave and maintained at 120 °C for 8 h. After cooling to room temperature, the precipitate was centrifuged and washed with deionized water and ethanol until the pH of the supernatant reached neutrality. The obtained solid was dried at 80 °C for 12 h, then calcined in a muffle furnace by heating to 500 °C at a rate of 5 °C·min^{-1} and holding for 2 h. After cooling to room temperature, the M-CoO_x catalysts were obtained. The catalyst is denoted as CoO_x, referring to the mixed-valence cobalt phase (Co^0 and $Co^{\delta+}$) generated after H_2 reduction and under working conditions, unless otherwise specified.

Na-promoted M-CoO_x catalysts were further prepared by an impregnation method. Specifically, 200 mg of M-CoO_x and an appropriate amount of Na_2CO_3 (corresponding to a Na loading of 1.0 wt%) were dispersed in a mixed solvent containing 500 μL of deionized water. The resulting suspension was ultrasonicated for 1 h and then aged at room temperature for 2 h. The sample was subsequently dried at 80 °C overnight and calcined at 300 °C for 2 h in a muffle furnace to obtain the Na-M-CoO_x catalyst.

Catalytic reaction

The catalytic performance was evaluated in a continuous fixed-bed reactor built by Xiamen HanDe Engineering Co., Ltd. Typically, 0.1 g of catalyst (40−60 meshes) was diluted with 0.5 g of SiC and

mounted inside the reactor. Before the reaction, the catalyst was reduced with a H_2 of 8 mL·min^{-1} at 300 °C for 2 h unless otherwise specified and then cooled to room temperature. The reactant gas mixture with an H_2/CO_2/Ar (volume ratio of 72/24/4) and a typical WHSV of 6000 mL·g_{cat}^{-1}·h^{-1} was introduced into the reactor and pressured to 3 MPa to start the reaction.

The products were analyzed with an online gas chromatograph (Ruimin GC-2060). Ar, CO, CO_2, and CH_4 were separated by a TDX-01 packed column and analyzed with a TCD detector. Hydrocarbon products were separated by Rt-Q-Bond and KB-PONA capillary columns, then analyzed with an FID detector. All connection lines between the reactor and GC were heated at 220 °C to gasify all the products.

The CO_2 was calculated by the following formula:

$$X_{CO_2}(\%)=\left(1-\frac{\left(A_{CO_2}/A_{Ar}\right)}{\left(A^0_{CO2}/A^0_{Ar}\right)}\right)*100\%$$

A_{CO2} and A_{Ar} represent the thermal conductivity detector (TCD) peak area of CO_2 and Ar during the reaction. A^0_{CO2} and A^0_{Ar} are the TCD peak areas of CO_2 and Ar recorded in a blank measurement.

CO selectivity in CO_2 hydrogenation was calculated separately, according to the following formula:

$$S_{CO}(\%)=\left(\frac{CO_{out}}{CO_{2_{in}}\text{-}CO_{2_{out}}}\right)*100\%$$

where CO_{2in}, CO_2/CO_{out} are CO_2/CO concentrations in the inlet and outlet gas flow.

The hydrocarbon selectivity in CO_2 hydrogenation was calculated using the formula:

$$S_{C_xH_y}(\%)=\left(\frac{x\left(C_xH_y\right)_{out}}{\sum_{n=1}^{\infty} nC_nH_y}\right)*100\%$$

In this equation, $(C_xH_y)_{out}$ corresponds to the individual hydrocarbon product at the outlet.

$$STY_i(\text{mmol}\cdot g_{cat}^{-1}\cdot h^{-1}) = X_{CO2} * F_{CO2} * S_i * 60/(22.4 * M_{cat} * 10^4)$$

where X_{CO2} denotes the conversion of CO_2. F_{CO2} denotes the CO_2 gas flow rate, and the unit is mL·min^{-1}. S_i denotes the selectivity of i, M_{cat} denotes the weight of the catalyst, and the unit is g.

$$\ln\frac{W_n}{n} = n\ln\alpha + \ln\frac{(1\text{-}\alpha)^2}{\alpha}$$

W_n is the mass fraction of the component with carbon number n; α is the chain growth factor.

The hydrocarbon selectivity and formation rates are presented on a carbon basis, i.e., the amount of CO_2 converted to a certain hydrocarbon molecule. The carbon balances are better than 95%.

Catalyst characterization

X-ray powder diffraction (XRD) measurements were conducted on a Rigaku Ultima IV diffractometer. The Cu Kα radiation (λ = 0.15 nm) generated at 40 kV and 30 mA was used as the X-ray source. High-Resolution Transmission Electron Microscopy (HRTEM) and Energy Dispersive X-ray Spectroscopy Mapping (EDS-Mapping) were carried out on a JEOL JEM-F200 field-emission transmission electron microscope operated at an accelerating voltage of 200 kV and a JEOL JEM-ARM300F2 cold field-emission transmission electron microscope operated at an accelerating voltage of 300 kV. The Scherrer-derived crystallite size and TEM-observed particle size are not directly equivalent, as the latter may be influenced by particle aggregation and sampling statistics. The Scherrer analysis is mainly used here to compare the relative size trends among different samples. Scanning Electron Microscope (SEM) images were obtained from the Hitachi UHR FE-SEM SU8220 instrument. The nitrogen adsorption and desorption isotherms were measured at the Micromeritics ASAP 2020 fully automatic surface area analyzer. Before the experiment, the samples were placed in a vacuum environment and treated for 4 h at 200 °C to eliminate gas impurities completely from the catalyst surface. The total specific surface area was determined after using the BET method, while the external surface area and micropore volume were derived from the t-plot method. The total pore volume was derived from a single-point measurement at $P/P_0 = 0.99$. The UV-vis absorption spectra were recorded on a Cary 5000 UV-Vis-NIR spectrophotometer (Agilent Technologies, USA) over the range of 200−800 nm with a scanning rate of 20 nm s^{-1}. The actual loading of Na, Co, and V on various catalysts was measured by inductively coupled plasma optical emission spectroscopy (ICP-OES) with a Varian ICP-OES 720.

H_2 temperature-programmed reduction (H_2-TPR) measurements were performed on a Beijing JWGB Instrument AMI-300. For H_2-TPR measurements, 50 mg of the sample was pretreated at 300 ℃ for 1 h under He flow to remove any absorbed ambient gas molecules on the catalyst surface. After cooling to 50 ℃, a 10 vol% H_2/Ar mixture with a rate of 30 mL min^{-1} was introduced into the reactor, and the temperature was raised from 50 to 700 °C at a temperature ramp of 10 °C min^{-1}. The consumption of H_2 was monitored by a thermal conductivity detector.

Ex situ X-ray photoelectron analysis (XPS) was performed with an Axis Ultra DLD (Kratos Tech.) equipment. The spectra were excited by a monochromatized Al Kα source (1486.6 eV) run at 15 kV and 10 mA. For the calibration measurement, the C 1s peak at 284.8 eV was used as a reference standard to

calibrate the binding energy. The used catalysts for characterization were passivated by a gas flow of 1 vol% O_2 in N_2 at room temperature for 30 min before being removed from the reactor. In situ diffuse reflectance infrared Fourier-transform spectroscopy (DRIFTS) was performed on a Bruker Vertex 70v equipped with a mercury cadmium telluride (MCT) detector. For the CO_2/H_2 co-feed reaction study, the catalysts were first reduced in flowing H_2 at 300 ℃ for 2 h. followed by purging with Ar at the same temperature for 30 min. After cooling the sample to 250 ℃, a background spectrum was collected from 900 to 4000 cm^{-1} with 64 scans and a resolution of 4 cm^{-1}. Subsequently, a gas mixture of CO_2/H_2 (24% CO_2, 72% H_2, and 4% Ar) was introduced into the reaction cell with a flow rate of 20 $mL \cdot min^{-1}$ to 2 MPa. Sample spectra were then acquired under the same scanning parameters as the background, recorded at 1 min intervals until spectral features stabilized.

Supplementary tables and figures

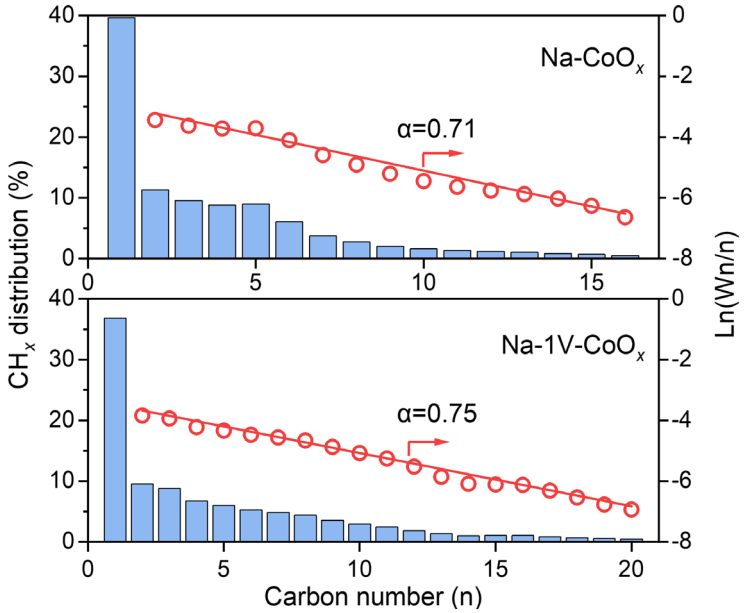

Fig. S1 The hydrocarbon distribution and ASF plots (C_2–C_{20}) of Na-CoO_x and Na-1V-CoO_x in CO_2 hydrogenation. Reaction conditions: 0.1 g, 250 °C, H_2/CO_2 = 3, 3 MPa, 6000 mL·$g_{cat.}^{-1}$·h^{-1}.

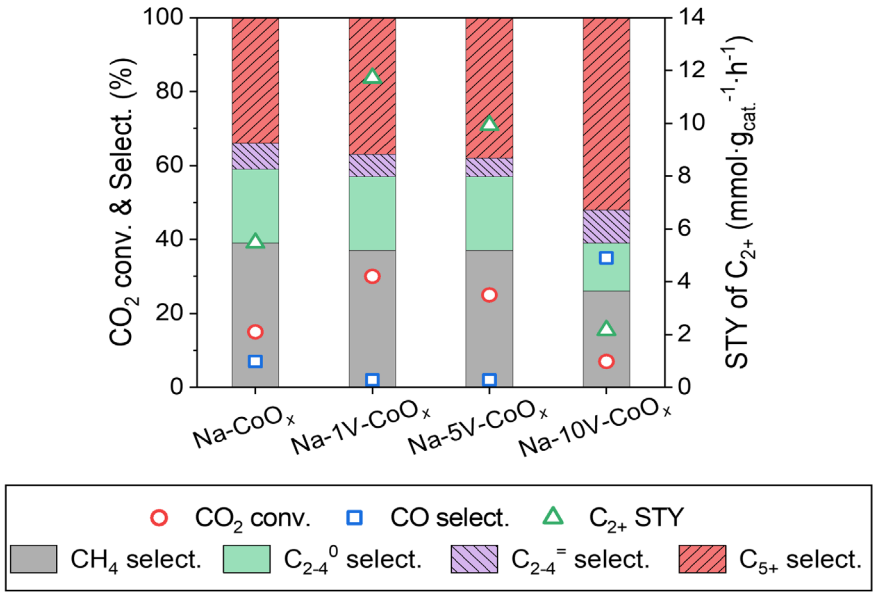

Fig. S2 Catalytic performance of CO_2 hydrogenation over Na-CoO_x and Na-*y*V-CoO_x catalysts (y = 1.0, 5.0, and 10 wt%). Reaction conditions: 0.1 g, 250 °C, H_2/CO_2 = 3, 3 MPa, 6000 $mL \cdot g_{cat.}^{-1} \cdot h^{-1}$.

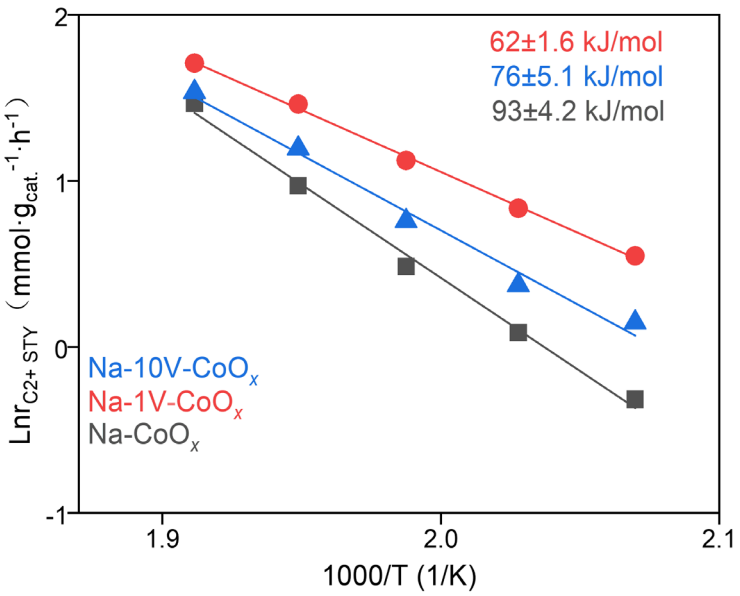

Fig. S3 Arrhenius plots for CO_2 hydrogenation over Na-CoO_x and Na-*y*V-CoO_x catalysts (y = 1.0 and 10 wt%). Reaction conditions: 0.1 g, 210-250 °C, H_2/CO_2 = 3, 3 MPa, 9000 mL·$g_{cat.}^{-1}$·h^{-1}.

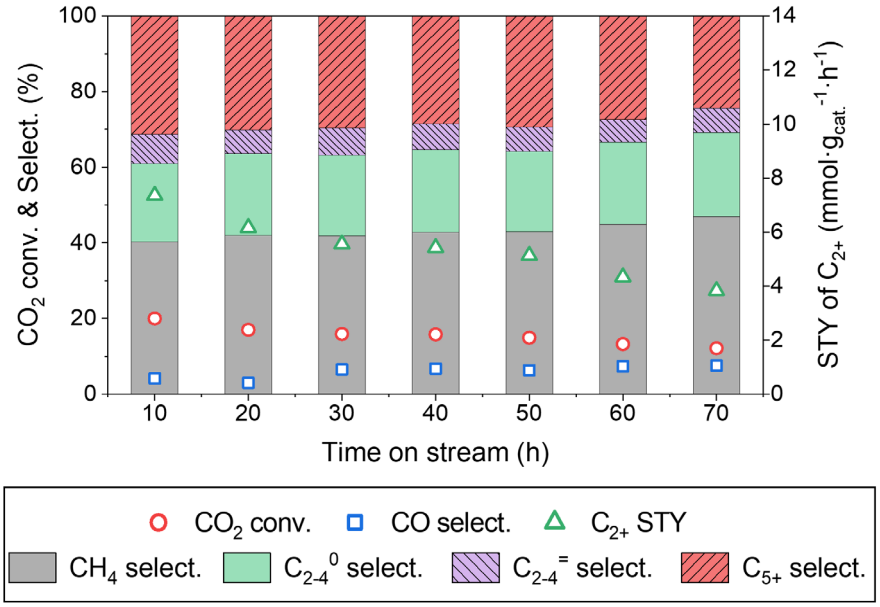

Fig. S4 Stability of Na-CoO_x in CO_2 hydrogenation. Reaction conditions: 0.1 g, 250 °C, H_2/CO_2 = 3, 3 MPa, 6000 mL·$g_{cat.}^{-1}$·h^{-1}.

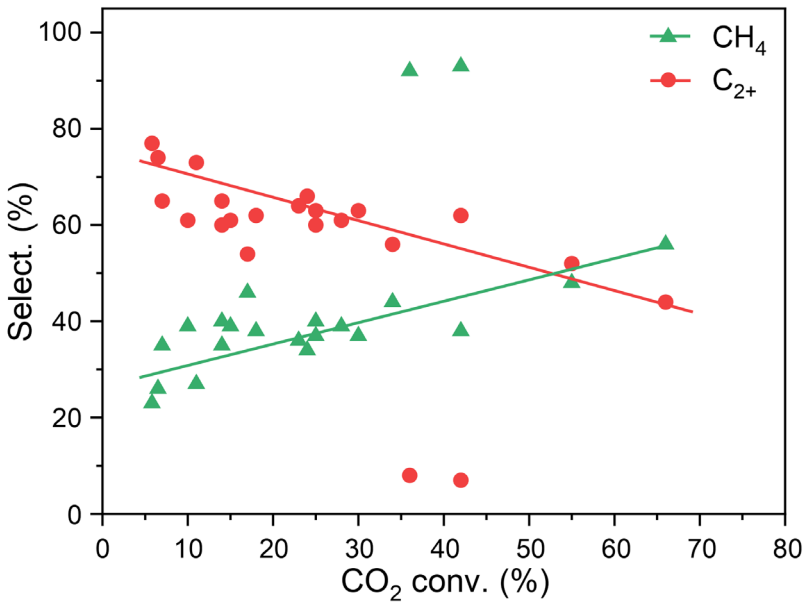

Fig. S5 CH_4, and C_{2+} selectivities as a function of CO_2 conversion over Co-based catalysts. Detailed reaction conditions and performances are listed in Table S2.

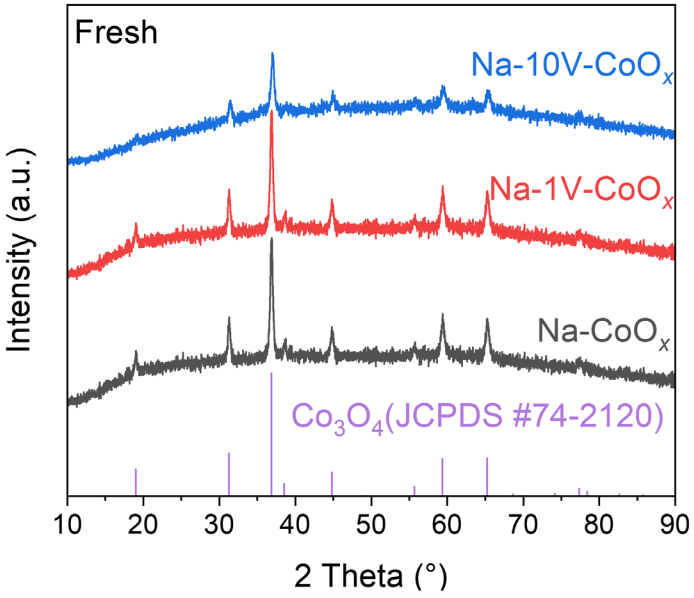

Fig. S6 XRD patterns of fresh Na-CoO_x and Na-*y*V-CoO_x catalysts (y = 1.0 and 10 wt%).

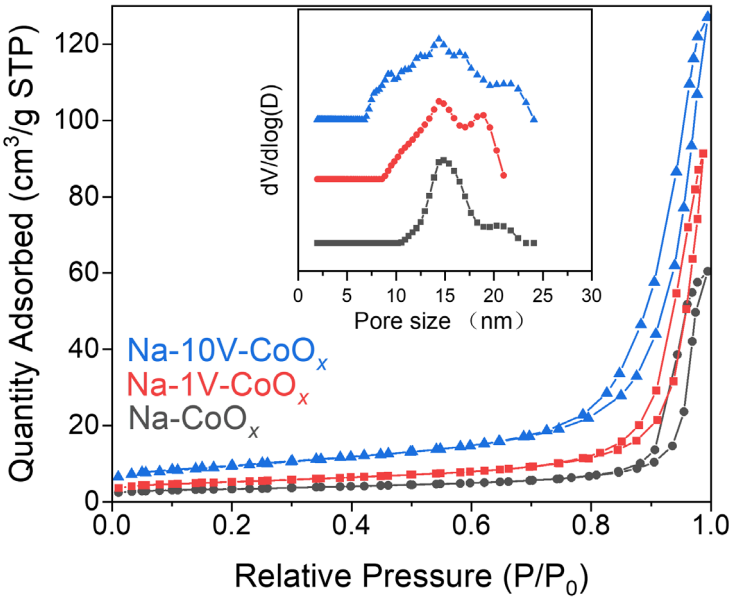

Fig. S7 Nitrogen adsorption-desorption isotherms of fresh Na-CoO_x and Na-*y*V-CoO_x catalysts (y = 1.0 and 10 wt%).

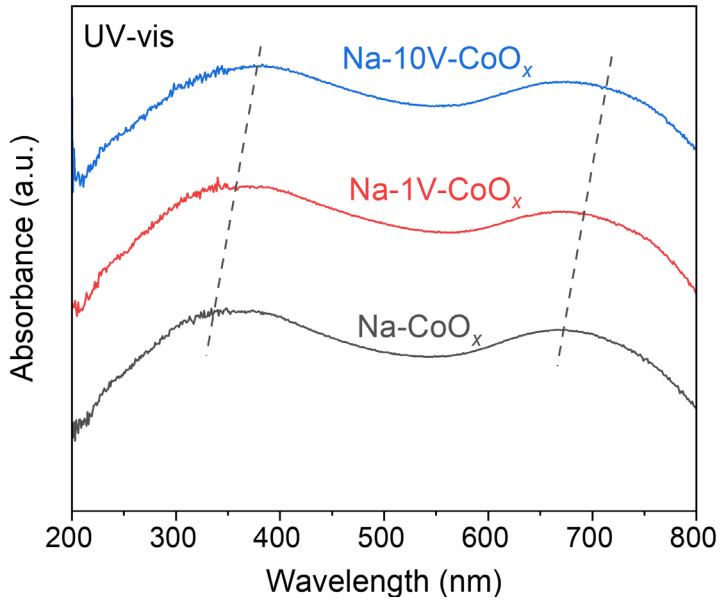

Fig. S8 Uv-vis profiles of fresh Na-CoO_x and Na-*y*V-CoO_x catalysts (y = 1.0 and 10 wt%).

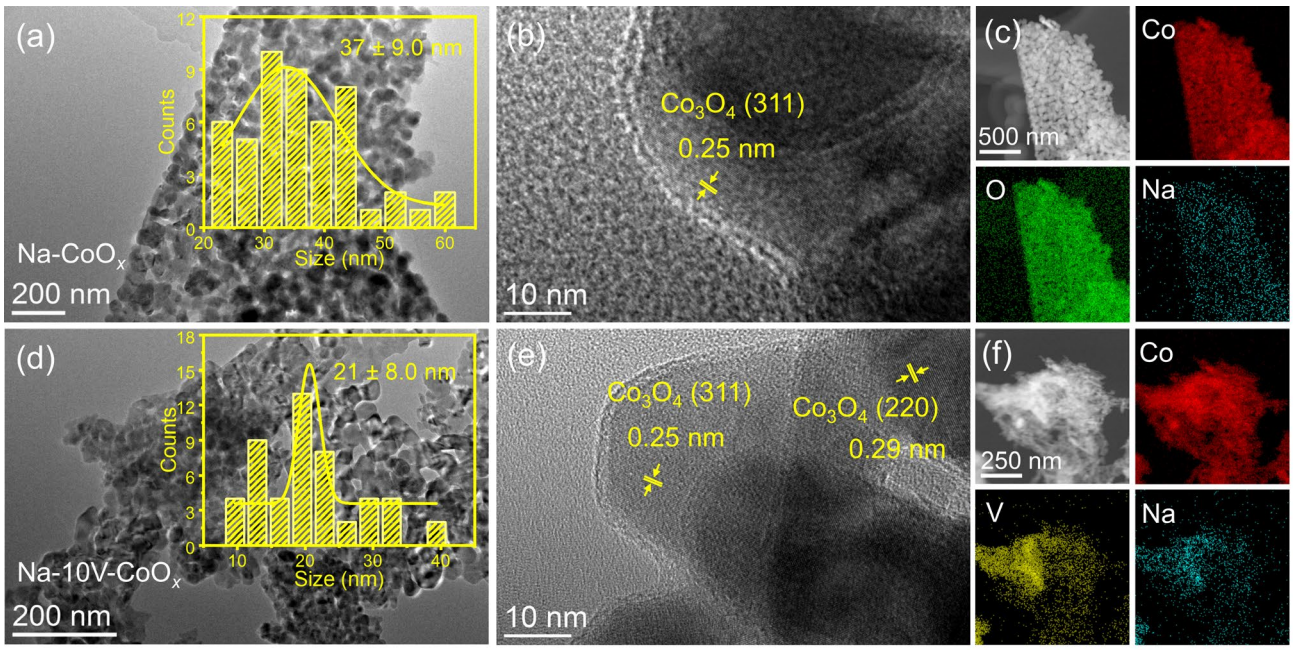

Fig. S9 HRTEM and STEM-EDS mapping of fresh (a-c) Na-CoO_x and (d-f) Na-10V-CoO_x catalysts.

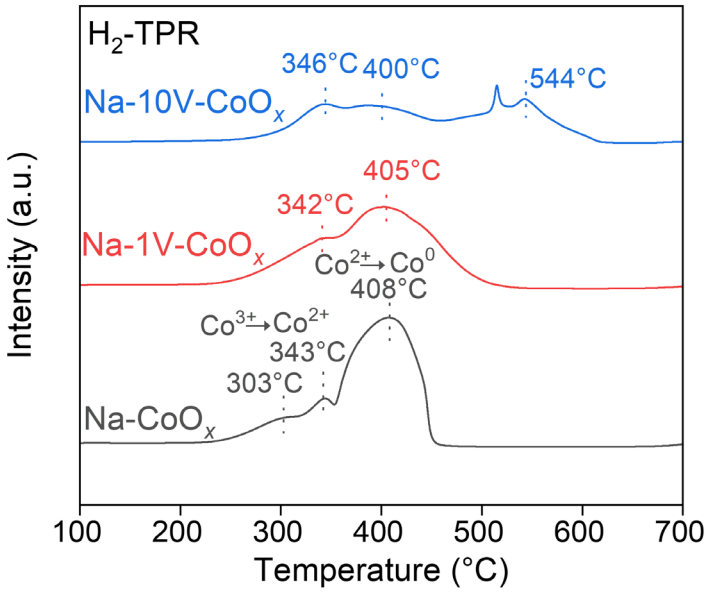

Fig. S10 (a) H_2-TPR spectra of fresh Na-CoO_x and Na-*y*V-CoO_x catalysts (y = 1.0 and 10 wt%).

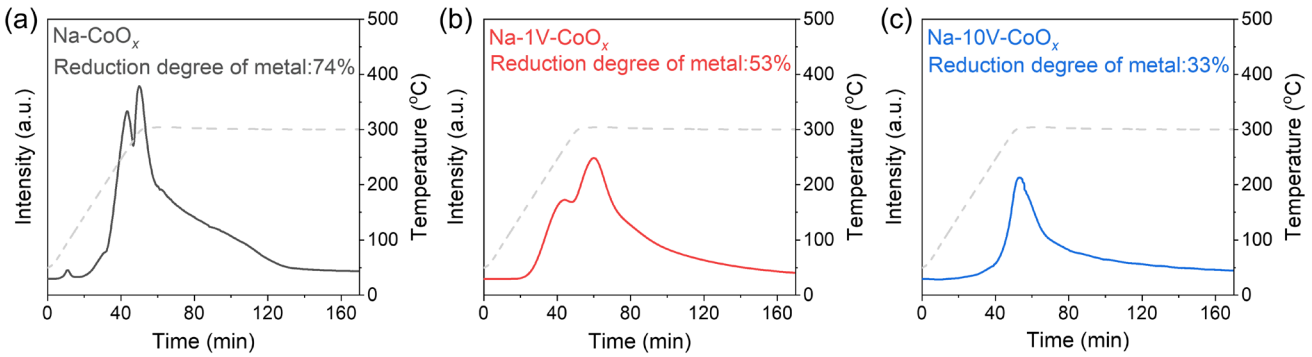

Figure S11 H_2-TPR profiles of (a) Na-CoO_x, (b) Na-1V-CoO_x, and (c) Na-10V-CoO_x catalysts. CuO was chosen as the standard sample to calibrate the H_2 consumption, and then the H_2 consumption of the catalyst was compared with it to determine the reduction degree of the metal.

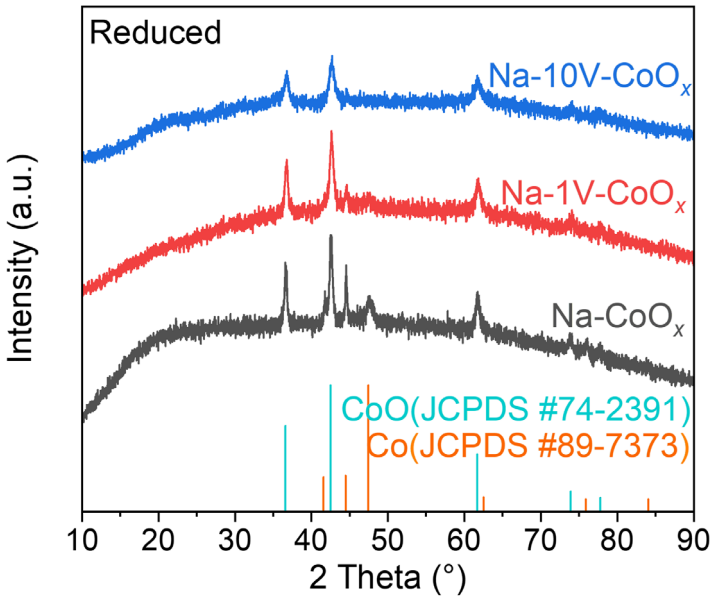

Fig. S12 (a) XRD patterns of reduced Na-CoO_x and Na-*y*V-CoO_x catalysts (y = 1.0 and 10 wt%).

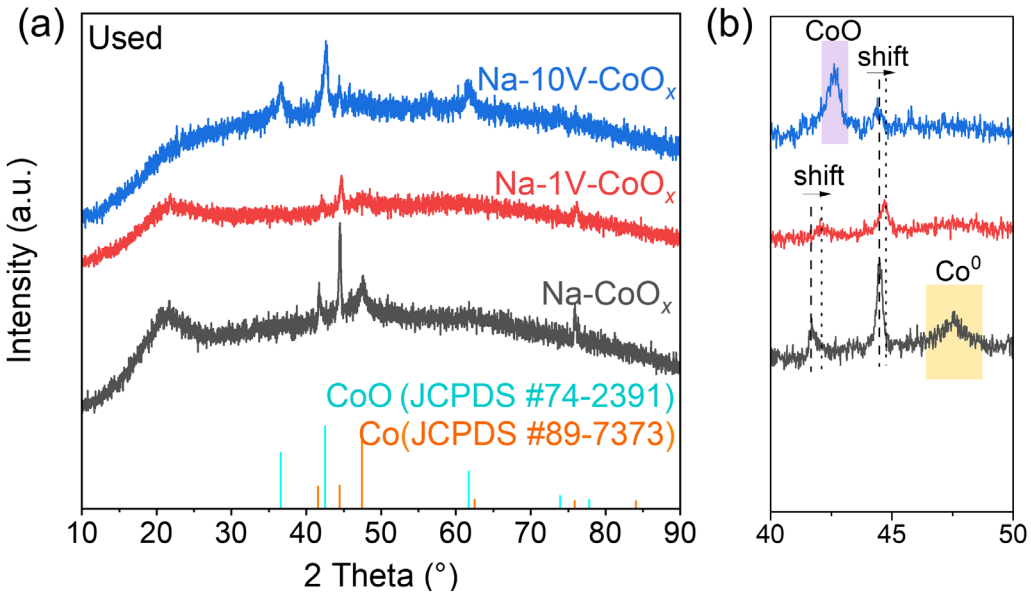

Fig. S13 (a) XRD patterns of used Na-CoO$_x$ and Na-*y*V-CoO$_x$ catalysts (y = 1.0 and 10 wt%). (b) Magnified XRD patterns in the 2-theta range of 40-50°.

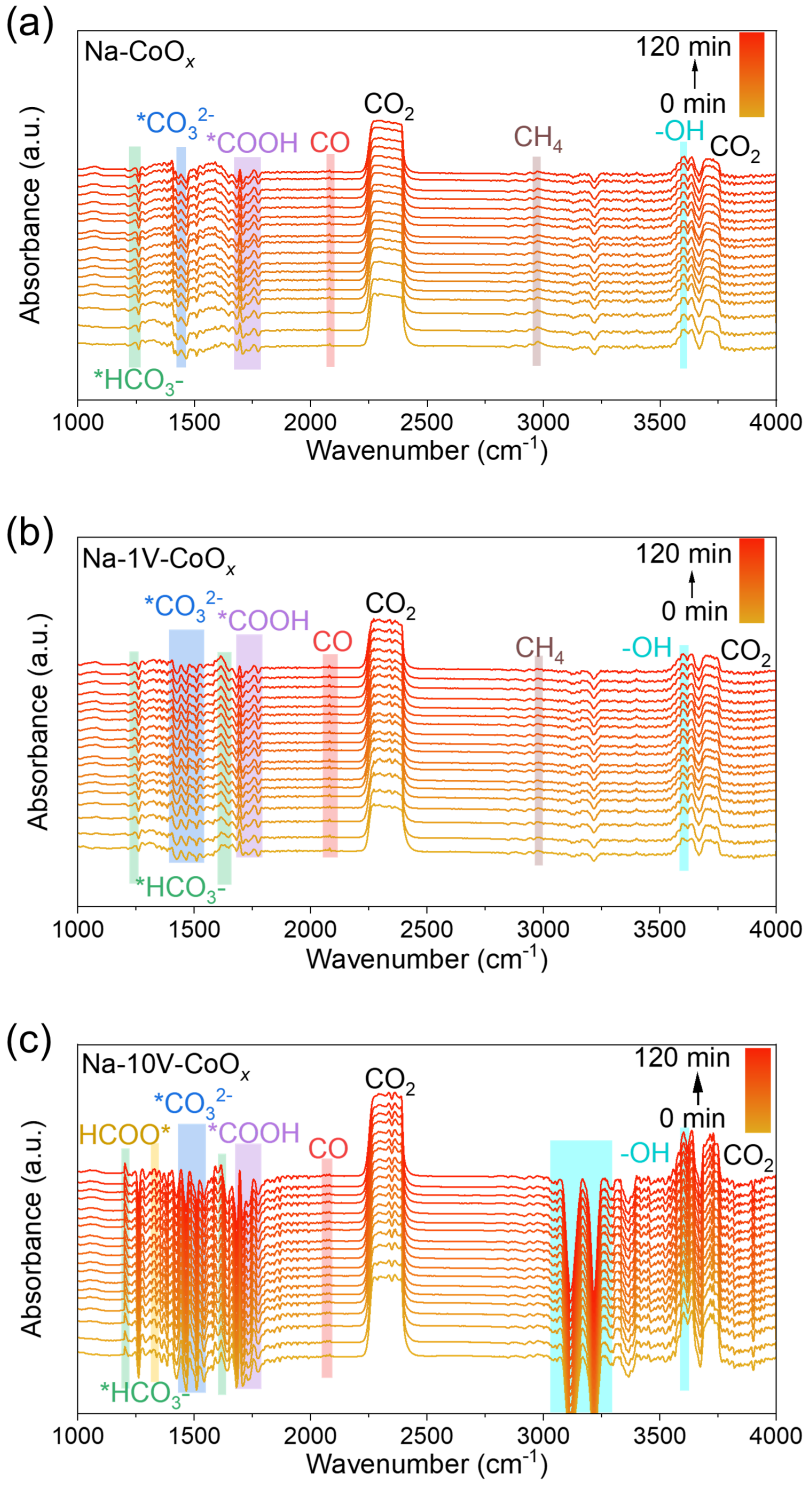

Fig. S14 *In-situ* DRIFTS during the CO_2 hydrogenation of (a) Na-CoO_x, (b) Na-1V-CoO_x, and (c) Na-10V-CoO_x.

Table S1 Statistics of Co and Fe-based catalysts for CO_2 hydrogenation to C_{2+} hydrocarbons.

Catalysts	Reaction condition				Catalytic performance						Ref.
	Reaction temp. (°C)	Reaction pressure (MPa)	H_2/CO_2	WHSV (mL·$g_{cat.}^{-1}$·h^{-1})	CO_2 conv. (%)	CO select. (%)	CH_4 select. (%)	C_{2-4} select. (%)	C_{5+} select. (%)	$C_{2+}H$ yield (%)	$C_{2+}H$ STY (mmol·$g_{cat.}^{-1}$·h^{-1})	
Na–CoCu/TiO_2	250	5	3	3,000	18	30	19	22	29	9.2	3.1	1
Na–$CoZrO_x$-8	270	4	3	4,000	70	0.1	43	19	39	40	17	2
K–$CoCuO_x$	300	3	3	6,000	34	10	25	44	21	22	14	3
Na-CoMn	270	4	3	4,000	64	0	45	22	33	35	14	4
$Na_{0.02}Fe_1Co_1$	320	3	3	4800	56	4.0	26	44	26	39	20	5
Na-CoMn-TiO_2	270	4	3	4,000	42	0	42	23	35	24	10	6
Co-TiO_2	220	2	2	1620	16	25	56	20	24	5.3	0.9	7
65Co–30Cu–5La	200	1	3	2000	35	0	65	15	20	12	2.6	8
Na-Co-SiO_2	300	1	3	18000	10	65	15	C_{2+}=20		2.0	3.8	9

Co/MnO_x	400	0.1	4	60000	12	93	7.0	\	\	\	\	10
$Co\text{-}Cu/CeZrO_x$	400	0.1	4	36000	45	100	\	\	\	\	\	11
Co	400	0.1	3	240000	40	100	\	\	\	\	\	12
Co/SiO_2	230	2.5	3	30000	5.1	55	35	CH_3OH=10				13
CoO	300	0.1	3	\	13	77	23	\	\	\	\	14
$Na\text{-}Co/SiO_2$	250	5	3	6000	22	26	38	10	CH_3OH=26		\	15
Co/MnO@PGC	200	3	3	15000	46	1.0	99	\	\	\	\	16
Na-FeZn	340	2.5	3	15000	38	15	13	47	40	33	18	17
FeCoK@C	320	3	3	18000	52	4.6	24	46	30	40	24	18
$FeCo@ZrO_2$	340	3	3	5000	45	18	20	63	17	36	19	19
$Na\text{-}1V\text{-}CoO_x$	250	3	3	6000	30	1.8	37	25	37	19	12	This work

Table S2. Detailed catalyst information, reaction conditions, and catalytic performance of all Co-based catalysts tested in this study.

Catalyst	Reaction conditions				CO_2 conv. (%)	CO select. (%)	CH_4 select. (%)	C_{2-4}^0 select. (%)	$C_{2-4}^=$ select. (%)	C_{5+} select. (%)	O/P	C_{2+} STY ($mmol \cdot g_{cat.}^{-1} \cdot h^{-1}$)
	H_2/CO_2	T (°C)	P (MPa)	WHSV ($mL \cdot g_{cat.}^{-1} \cdot h^{-1}$)								
CoO_x	3	250	3	6000	42	0.4	93	7.0	0	0	0	2.8
1V-CoO_x	3	250	3	6000	36	0.6	92	8.0	0	0	0	1.8
Na-CoO_x	3	250	3	6000	15	6.5	39	20	7	34	0.4	5.5
Na-1In-CoO_x	3	250	3	6000	17	3.4	46	24	2	28	0.1	5.7
Na-1Ga-CoO_x	3	250	3	6000	18	5.1	38	14	8	40	0.6	6.8
Na-1Mo-CoO_x	3	250	3	6000	24	11	34	17	12	37	0.7	9.1
Na-1Mn-CoO_x	3	250	3	6000	28	2.2	39	17	8	36	0.5	11
Na-1V-CoO_x	3	250	3	6000	30	1.8	37	20	6	37	0.3	12
Na-5V-CoO_x	3	250	3	6000	25	2.3	37	20	5	38	0.3	10
Na-10V-CoO_x	3	250	3	6000	6.5	35	26	13	9	52	0.7	2.2
Na-1V-CoO_x	3	210	3	6000	5.8	7.9	23	20	7	50	0.4	2.7

Na-1V-CoO_x	3	230	3	6000	11	7.5	27	18	11	44	0.6	4.8
Na-1V-CoO_x	3	270	3	6000	55	0.7	48	20	2	30	0.1	18
Na-1V-CoO_x	3	290	3	6000	66	0.5	56	18	2	24	0.1	19
Na-1V-CoO_x	3	250	1	6000	14	11	35	17	10	38	0.6	5.2
Na-1V-CoO_x	3	250	2	6000	23	3.3	36	19	9	36	0.5	9.2
Na-1V-CoO_x	3	250	4	6000	34	1.1	44	24	4	28	0.2	12
Na-1V-CoO_x	3	250	3	3000	42	0	38	10	6	46	0.6	17
Na-1V-CoO_x	3	250	3	9000	14	4.6	40	20	6	35	0.3	5.2
Na-1V-CoO_x	3	250	3	12000	10	6.2	39	23	6	32	0.3	3.7
Na-1V-CoO_x-reduced at 250 ^oC	3	250	3	6000	7.0	80	35	13	12	40	0.9	0.6
Na-1V-CoO_x-reduced at 350 ^oC	3	250	3	6000	25	2.6	40	23	5	32	0.2	9.4

Table S3 Textural properties of Na-CoO_x and Na-*y*V-CoO_x catalysts (y = 1.0 and 10 wt%).

Catalysts	Co loading (wt %)[a]	Na loading (wt %)[a]	V loading (wt %)[a]	Surface Area (m^2/g)[b]	Pore Volume (cm^3/g)[c]	Pore Size (nm)[c]	Particle Size (nm)[e]	Particle Size (nm)[f]	Phase content[f]	Degree of reduction[g]
Na-CoO_x-fresh	73	0.9	0	11	0.1	29	37	55	Co_3O_4	74%
Na-1V-CoO_x-fresh	71	0.9	0.9	18	0.1	27	25	35	Co_3O_4	53%
Na-10V-CoO_x-fresh	62	0.9	9.5	32	0.2	22	21	30	Co_3O_4	33%
Na-CoO_x-used	\	\	\	\	\	\	65	68	Co^0	\
Na-1V-CoO_x-used	\	\	\	\	\	\	44	46	Co^0	\
Na-10V-CoO_x-used	\	\	\	\	\	\	30	37	CoO and Co^0	\

[a] Determined by inductively coupled plasma (ICP) analysis.

[b] Surface area was calculated by using the BET method.

[c] Pore volume and pore size were evaluated by the BJH method.

[e] Determined by TEM analysis.

[f] Determined by XRD analysis.

[g] Determined by H_2-TPR analysis.

Table S4 Curve fitting analysis results of XPS for used CoO_x, 1V-CoO_x, Na-CoO_x, and Na-*y*V-CoO_x catalysts (y = 1.0 and 10 wt%).

Catalysts	Component		spectral shape	FWHM	Position (eV)
CoO_x-used	Co $2p_{3/2}$	Co^0	LG (95)	0.9	778.1
		$Co^{\delta+}$	LG (0)	2.3	779.8
		$Co^{2+}(Co_3O_4)$	LG (86)	2.5	781.0
	O 1s	M-O	LG (53)	1.3	529.6
		C-O	LG (0)	1.6	531.3
		C=O	LG (34)	2.5	532.4
	C 1s	C-C	LG (55)	1.2	284.8
		C-O-C	LG (59)	2.5	286.6
		O-C=O	LG (0)	1.5	289.2
Na-CoO_x-used	Co $2p_{3/2}$	Co^0	LG (87)	1.0	778.1
		$Co^{\delta+}$	LG (0)	3.1	779.9
		$Co^{2+}(Co_3O_4)$	LG (0)	3.2	781.8
	O 1s	M-O	LG (52)	1.2	529.6
		C-O	LG (0)	1.5	531.4
		C=O	LG (48)	1.9	531.9
	C 1s	C-C	LG (55)	1.2	284.8
		C-O-C	\	\	\
		O-C=O	\	\	\
	Na 1s	Na^+	LG (39)	1.7	1071.5
1V-CoO_x-used	Co $2p_{3/2}$	Co^0	LG (95)	1.4	778.5
		$Co^{\delta+}$	LG (0)	2.0	780.1
		$Co^{2+}(Co_3O_4)$	LG (0)	2.4	781.9
	O 1s	M-O	LG (37)	1.4	530.3
		C-O	LG (0)	1.5	531.6
		C=O	LG (71)	2.0	532.3
	C 1s	C-C	LG (35)	1.1	284.8
		C-O-C	LG (73)	2.0	285.7
		O-C=O	LG (29)	2.2	289.4

	V 2p$_{3/2}$	V^{3+}	LG (93)	1.9	514.7
		V^{4+}	LG (0)	1.9	516.2
		V^{5+}	LG (43)	1.9	517.4
Na-1V-CoO$_x$-used	Co 2p$_{3/2}$	Co^{0}	LG (0)	1.3	777.7
		$Co^{\delta+}$	LG (0)	2.6	779.7
		$Co^{2+}(Co_3O_4)$	LG (0)	3.5	781.2
	O 1s	M-O	LG (0)	1.9	529.5
		C-O	LG (51)	1.5	531.4
		C=O	LG (0)	3.5	534.8
	C 1s	C-C	LG (69)	1.1	284.8
		C-O-C	\	\	\
		O-C=O	\	\	\
	Na 1s	Na^{+}	LG (57)	1.6	1071.2
	V 2p$_{3/2}$	V^{3+}	LG (85)	1.5	514.7
		V^{4+}	LG (18)	2.8	516.1
		V^{5+}	LG (0)	1.8	516.8
Na-10V-CoO$_x$-used	Co 2p$_{3/2}$	Co^{0}	LG (96)	2.6	777.9
		$Co^{\delta+}$	LG (0)	2.9	778.0
		$Co^{2+}(Co_3O_4)$	LG (0)	3.5	781.5
	O 1s	M-O	LG (46)	1.3	529.7
		C-O	LG (43)	1.8	531.4
		C=O	\	\	\
	C 1s	M-C	LG (98)	0.8	283.1
		C-C	LG (27)	1.3	284.8
		C-O-C	LG (0)	1.4	286.2
		O-C=O	LG (0)	2.1	288.7
	Na 1s	Na^{+}	LG (37)	1.6	1071.4
	V 2p$_{3/2}$	V^{3+}	LG (85)	1.8	514.3
		V^{4+}	LG (0)	2.3	516.1
		V^{5+}	LG (0)	2.0	517.6

Table S5. Product formation rates and surface $Co^0/Co^{\delta+}$ ratios over a series of Co-based catalysts

Catalysts	$Co^0/Co^{\delta+}$	$C_{2+}H$ STY ($mmol \cdot g_{cat.}^{-1} \cdot h^{-1}$)
CoO_x	0.56	2.8
1V-CoO_x	0.53	1.8
Na-CoO_x	0.47	5.5
Na-1V-CoO_x	0.42	12
Na-10V-CoO_x	0.37	2.2

References

1 Z. Shi, H. Yang, P. Gao, X. Chen, H. Liu, L. Zhong, H. Wang, W. Wei and Y. Sun, *Chin. J. Catal.*, 2018, **39**, 1294-1302.

2 S. S. Bibi, H. Jo, J. R. Sugiarto, S. Ahmed, M. Irshad, W. Yoon and J. Kim, *J. Energy Chem.*, 2025, **108**, 769-784.

3 M. Wang, S. Guo, S. Yan, Z. Wang, G. Zhang, H. Gao, M. Zhang, K. Bian, J. Liu, X. Nie, J. Zeng, C. Song and X. Guo, *J. Am. Chem. Soc.*, 2025, **147**, 42051-42060.

4 H. Jo, M. K. Khan, M. Irshad, M. W. Arshad, S. K. Kim and J. Kim, *Appl. Catal. B: Environ.*, 2022, **305**, 121041.

5 T. Li, H. Zhao, L. Guo, G. Liu, J. Wu, T. Xing, T. Li, Q. Liu, J. Sui, Y. Han, J. Liang, Y. He and N. Tsubaki, *ACS Catal.*, 2025, **15**, 1112-1122.

6 H. Jo, H.-J. Chun, J. R. Sugiarto, M. K. Khan, M. Irshad, W. Yoon, S. K. Kim and J. Kim, *Appl. Catal. B: Environ.*, 2024, **359**, 124457.

7 C. Scarfiello, K. Soulantica, S. Cayez, A. Durupt, G. Viau, N. Le Breton, A. K. Boudalis, F. Meunier, G. Clet, M. Barreau, D. Salusso, S. Zafeiratos, D. P. Minh and P. Serp, *J. Catal.*, 2023, **428**, 115202.

8 V. N. Borshch, S. Ya. Zhuk, E. V. Pugacheva, T. Duncan Dipheko, D. E. Andreev, Y. A. Agafonov and O. L. Eliseev, *Mendeleev Commun.*, 2023, **33**, 55-57.

9 M. Wang, G. Zhang, J. Zhu, W. Li, J. Wang, K. Bian, Y. Liu, F. Ding, C. Song and X. Guo, *Chem. Eng. J.*, 2022, **446**, 137217.

10 H. Kang, R. Cao, Y. Zhang, X. Wang, L. Li, W. Chu, R. Zhang, S. Perathoner, G. Centi and Y. Liu, *Nat. Commun.*, 2026, **17**, 3604.

11 A. V. Jagtap, M. K. Bamnia, A. Maibam, J. P. Bajpai, S. Gupta, S. K. Thomas, N. B. Dabke and C. P. Vinod, *Chem. Eng. J.*, 2025, **508**, 160705.

12 X. Chang, C. Yu, C. Yang, H. Xie, S. Xia, Z. Fang, J. Li, S. Zhang, F. Liu, T. Wang, Y. Tan, X. Chen, S. Shi, Q. Guo, Q. Xu, J. Hu, H. Ding, C. Huang, C. Zhou, J. Zhu, X. Yang and W. Yang, *J. Am. Chem. Soc.*, 2025, **147**, 16164-16170.

13 X. Zhou, G. A. Price, G. J. Sunley and C. Copéret, *Angew. Chem. Int. Ed.*, 2023, **135**, e202314274.

14 K. Li, X. Li, L. Li, X. Chang, S. Wu, C. Yang, X. Song, Z.-J. Zhao and J. Gong, *JACS Au*, 2023, **3**, 508-515.

15 S. Zhang, Z. Wu, X. Liu, Z. Shao, L. Xia, L. Zhong, H. Wang and Y. Sun, *Appl. Catal. B: Environ.*, 2021, **293**, 120207.

16 W.-G. Cui, X.-Y. Zhuang, Y.-T. Li, H. Zhang, J.-J. Dai, L. Zhou, Z. Hu and T.-L. Hu, *Appl. Catal. B: Environ.*, 2021, **287**, 119959.

17 Z. Zhang, H. Yin, G. Yu, S. He, J. Kang, Z. Liu, K. Cheng, Q. Zhang and Y. Wang, *J. Catal.*, 2021, **395**, 350-361.

18 M. Zhang, L. Zhang, M. Wang, G. Zhang, C. Song and X. Guo, *Chin. J. Catal.*, 2025, **68**, 366-375.

19 F. Xu, D. Yang, D. Jin, X. Meng, R. Zhao, W. Dai and Z. Xin, *Ind. Eng. Chem. Res.*, 2024, **63**, 20800-20811.